Overcoming the Cut-Off Charge Transfer Bandgaps at the PbS Quantum Dot Interface

*Ala'a O. El-Ballouli, Erkki Alarousu, Ahmad R. Kirmani, Aram Amassian, Osman M. Bakr, and Omar F. Mohammed**

Light harvesting from large size of semiconductor PbS quantum dots (QDs) with a bandgap of less than 1 eV is one of the greatest challenges precluding the development of PbS QD-based solar cells because the interfacial charge transfer (CT) from such QDs to the most commonly used electron acceptor materials is very inefficient, if it occurs at all. Thus, an alternative electron-accepting unit with a new driving force for CT is urgently needed to harvest the light from large-sized PbS QDs. Here, a cationic porphyrin is utilized as a new electron acceptor unit with unique features that bring the donor–acceptor components into close molecular proximity, allowing ultrafast and efficient electron transfer for QDs of all sizes, as inferred from the drastic photoluminescence quenching and the ultrafast formation of the porphyrin anionic species. The time-resolved results clearly demonstrate the possibility of modulating the electron transfer process between PbS QDs and porphyrin moieties not only by the size quantization effect but also by the interfacial electrostatic interaction between the positively charged porphyrin and the negatively charged QDs. This approach provides a new pathway for engineering QD-based solar cells that make the best use of the diverse photons making up the Sun's broad irradiance spectrum.

1. Introduction

One of the most important scientific and technological challenges of this century is the design of cost-effective next-generation photovoltaics (PVs) that operate efficiently over the broad solar irradiance spectrum range. Quantum dot (QD) solar cells,[1] especially those based on PbS QDs, have emerged as promising candidates because of QDs' size-tunable bandgaps (E_g), high absorptivity coefficients, solution-processability, and facile synthesis. Moreover, these QDs exhibit a unique ability to increase the photon conversion efficiency (PCE) beyond the theoretical Shockley–Quiesser (S–Q) limit via processes such as multiple exciton generation (MEG) and hot-carrier extraction.[2–4] These features of PbS QDs have enabled the engineering of various single-junction PV device architectures based on this material;[5–7] in addition, researchers have elucidated the charge transfer (CT) rates between PbS QDs and various acceptor moieties[8–11] to optimize their PV performance. Additionally, researchers attempting to fabricate tandem solar cells based on the size-quantization effect of PbS QDs have thus far successfully utilized QDs with E_g values of 1.6 and 1.0 eV to boost the PCEs.[12,13] Similarly, because of the additional driving force of quantum funneling, researchers have enhanced the PCE by employing a graded device architecture using PbS QDs with intermediate E_g values between 1.35 and 1.06 eV.[14] Although the use of larger QDs (with smaller E_g values) remains necessary and a key component to improve the device performance by multi-junction solar cells, most of the studies reported to date have demonstrated that only small PbS QDs (core diameter ≤ 4.3 nm, $E_g \geq 1.0$ eV) exhibit effective CT to common electron scavengers, such as TiO_2 nanoparticles,[15] SnO_2 nanoparticles,[16] PCBM,[11,17] and methyl viologen,[18] which is explained by such QDs exhibiting type II interfacial band alignments. These findings are further supported by a considerable reduction in the device PCE when QDs with larger diameters are used;[19,20] thus limiting the energy harvested from the Sun's broad spectrum.

In this work, we report a key variable component—specifically, electrostatic interaction—as a new driving force for CT at QD interfaces. Porphyrin-based electron acceptors were chosen for this study because of their wide use in PVs, their suitable reduction potentials,[21] and their peripheral substituents' versatility. The presence or absence of electrostatic interactions between the negatively charged QD surface and the positively or neutrally charged porphyrin derivatives enable the CT to be tuned from highly efficient and ultrafast (<120 fs) to nearly absent (**Scheme 1**). We demonstrate this tuning effect by manipulating these key parameters. As a result, we have extended the effective QD size for CT to include most of the near-infrared spectral region, reaching beyond the previously reported cut-off CT bandgaps for PbS QDs.

A. O. El-Ballouli, Dr. E. Alarousu, A. R. Kirmani, Prof. A. Amassain, Prof. O. M. Bakr, Prof. O. F. Mohammed
Division of Physical Sciences and Engineering
Solar and Photovoltaics Engineering Research Center
King Abdullah University of Science and Technology (KAUST)
Thuwal 23955-6900, Saudi Arabia
E-mail: omar.abdelsaboor@kaust.edu.sa

DOI: 10.1002/adfm.201504035

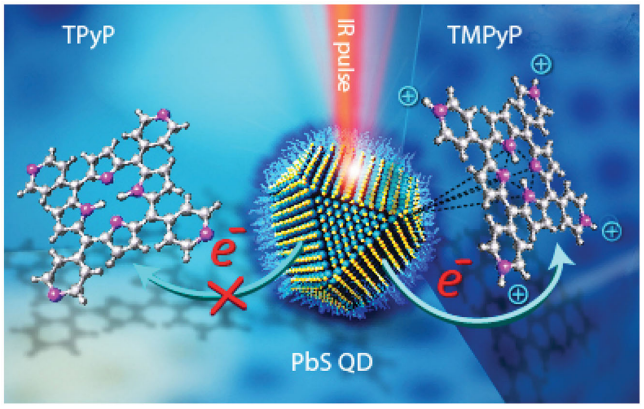

Scheme 1. The presence and absence of the CT process upon IR-pulse excitation from PbS QDs to TMPyP and TPyP, respectively.

2. Results and Discussion

2.1. Negatively Charged PbS QDs in Polar Medium

For this study, halide-passivated PbS QDs were prepared according to the method of Ip et al.,[5] followed by the ligand exchange of oleic acid ligands for 1-thioglycerol (TG) and dispersion in dimethyl sulfoxide (DMSO), as previously reported.[22] Further synthetic details are available in the Supporting Information. Notably, the halide treatment step (via $CdCl_2$)[5,23] was critical for better passivation of the surface, thus preserving the QDs' carrier lifetime after ligand exchange (**Figure 1**A). Without $CdCl_2$-treatment, the QDs showed lower photoluminescence and an increased recovery (recombination of charge carriers) due to trap states and imperfectly passivated surface upon ligand exchange. The ligand exchanged $CdCl_2$-treated QDs were characterized by X-ray photoelectron spectroscopy (XPS) which confirmed the binding of Cd, Cl, and TG to the PbS QDs (Figure 1C,D, and Table S1, Supporting Information), in good agreement with previous reports.[5,22] Transmission electron microscopy (TEM) and dynamic light scattering (DLS) measurements showed the maintenance of a uniform spherical shape and size distribution (Figure S2, Table S2, Supporting Information). Further, Zeta-potential measurement (Figure 1B) revealed a negatively charged surface for these QDs, in agreement with previous report by Sargent and co-workers.[22] It is worth pointing out that a possible explanation for the more negative values obtained with our QDs could be the extra passivation step, in which Cl^- ions were proven to constitute a higher percentage than Cd^{+2} ions, as indicated clearly in our XPS measurements (Table S1, Supporting Information). We synthesized QDs with different first excitonic absorption peaks (840, 1000, 1300, 1550 nm) corresponding to E_g between 1.48–0.80 eV. Herein, we refer to the QD samples based on the wavelength of the $1S_h \rightarrow 1S_e$ transition; e.g., the sample with a $1S_h \rightarrow 1S_e$ peak at 840 nm is named PbS-840.

2.2. PbS QDs/Cationic Porphyrin Interface

Figure 2 shows the changes in the steady-state absorption and photoluminescence (PL) spectra of PbS-840 and PbS-1300 upon the addition of different concentrations of the positively charged free-base porphyrin 5,10,15,20-tetra(*N*-methyl-4-pyridyl)porphyrin (TMPyP), whose structure and absorption spectrum are depicted in Figure S3A of the Supporting Information. The successive addition of TMPyP resulted in efficient quenching of the PL of the QDs. This result suggests that photoinduced CT occurs between the QDs as the donor and TMPyP as the acceptor. It is worth pointing out that although fluorescence quenching could also be achieved by energy transfer, we rule out this mechanism here on the basis of the lack of spectral overlap between the absorption of TMPyP and the emission of QDs. For PbS-840, the addition of 0.2×10^{-3} M TMPyP reduced the PL emission to nearly nil and resulted in a slight blue shift of both the first exciton absorption peak (approximately 15 nm) and the PL peak (approximately 12 nm). These spectral shifts may originate from modifications in the electronic density and confinement energy of the QDs, which are characteristic of the ground-state complex between a fluorophore and a quencher,[24,25] in agreement with previous reports.[11] Unlike our previous study between oleic acid-capped PbS QDs and PCBM,[11] large TG-capped QDs (PbS-1300) exhibit complete PL quenching with TMPyP (Figure 2). Although the extents of the spectral shifts were negligible compared to those of PbS-840, the significant PL quenching implies efficient electronic coupling between TMPyP and PbS-1300 in the excited state. The minimized spectral shifts upon TMPyP addition to larger QDs could be the result of the lessened electronic coupling in the ground state (Figure S8, Supporting Information) because of the decreased free-energy driving force ($-\Delta G$) for the CT (Figure S3B, Supporting Information). It is worth mentioning that the energy levels of the QDs were estimated with the aid of ultraviolet photoelectron spectroscopy (UPS) measurements to take into account the effect of the ligand-induced modifications on the absolute energy levels of the QDs.[26] Interestingly, drastic PL quenching was also observed upon the addition of TMPyP to PbS-1550 (E_g = 0.8 eV, core diameter ≈ 6 nm, Figure S4, Supporting Information). Importantly, this is the first time to report CT from such size of PbS QDs to molecular acceptor. A further consideration for donor–acceptor systems in the solution phase is whether PL quenching occurs via (1) static quenching, whereby a nonluminescent ground-state complex is formed, and/or (2) dynamic quenching, which involves collision. In this regard, the Stern–Volmer (SV) plots of small and large QDs revealed upward curvatures (Figure S5, Supporting Information), thus indicating the incorporation of both quenching mechanisms depending on the [TMPyP].[27,28]

Next, we employed femtosecond transient absorption (fs-TA) spectroscopy to study the ground-state bleach (GSB) dynamics upon bandgap excitation of the QDs. Because the GSB signal is directly associated with the electron population in the conduction band, we used it as a convenient probe to follow the CT and charge recombination (CR) dynamics at the QD interface. In particular, in addition to probing the formation of the porphyrin anionic species, we used the GSB signal to follow the charge recombination dynamics resulting from the CT process. The TA measurements of different PbS QD sizes were recorded following laser pulse excitation at approximately 1.3 times the bandgap to avoid any contribution from the scattered light in the GSB signal, thus assuring high-quality data and accurate dynamics for the CT process. Additionally, low pump energies

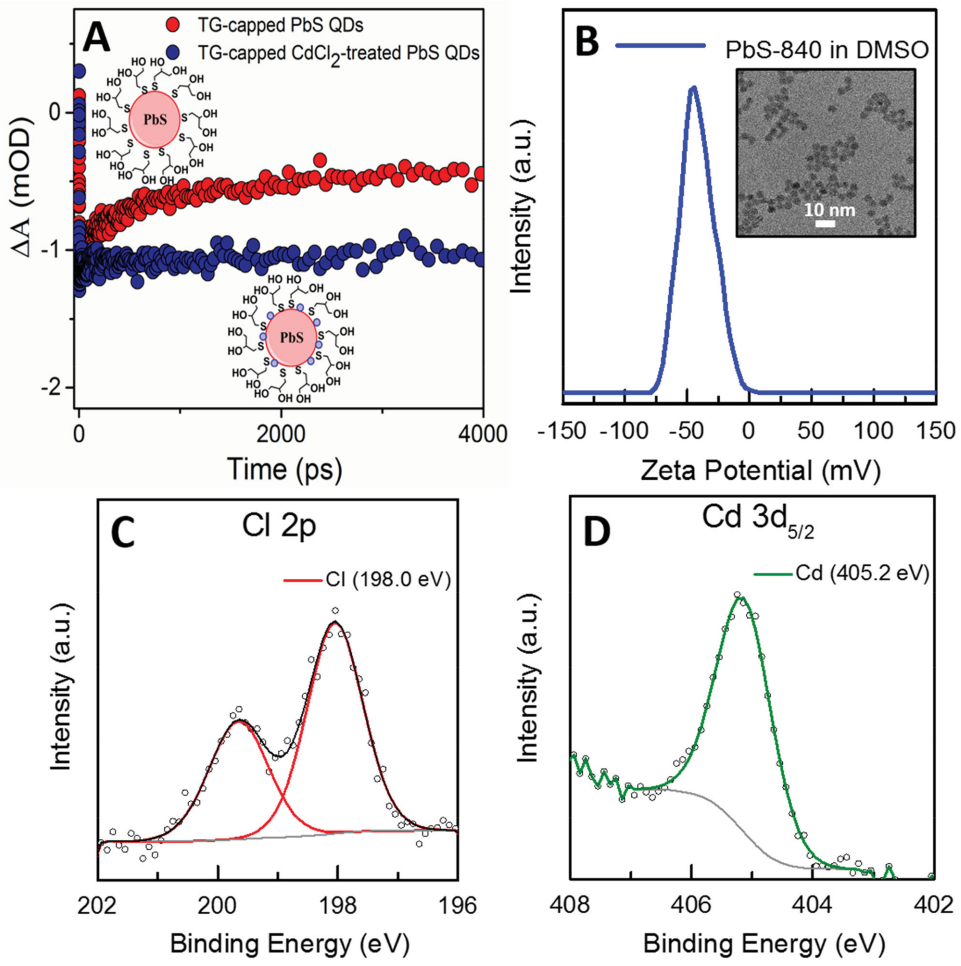

Figure 1. A) fs-TA kinetics traces at the GSB of similar-sized PbS QDs (PbS-1000) after ligand exchange to TG. Upon $CdCl_2$-treatment, the QDs show acceptable recovery kinetics after ligand exchange. B) Zeta-potential measurement of TG-capped $CdCl_2$-treated PbS QDs with a representative TEM image in the inset. C,D) XPS spectrum of PbS QD film showing Cl and Cd peaks enlarged, a survey XPS spectrum is available in the Supporting Information.

were maintained, with an average number of photons absorbed per QD less than 0.2, to ensure single-photon absorption and prevent contributions from Auger decay pathways.[29] Further details of the TA experimental apparatus and conditions are provided in the Supporting Information. **Figure 3**A shows the fs-TA spectra of large QDs (PbS-1300) recorded as [TMPyP] was increased. The pristine PbS QDs exhibited a very small decay (<15%) of the GSB on the picosecond (ps) time scale, which is attributed to state trapping (which lies just below the first confined electron state);[30] these results are consistent with those of previous reports[4,10] and indicate that most excited QDs are in long-lived single exciton states under these experimental conditions. The addition of TMPyP to solutions of PbS QDs accelerates the GSB recovery on the picosecond time scale. The boosted bleaching recoveries suggest the presence of an alternate deactivation pathway for the separated charges: CR following a CT process. On the basis of the energy-band alignments shown in Figure S3B of the Supporting Information, assisted by electrostatic interaction between the negatively charged QDs surface and the positively charged molecular acceptor, we attribute the exciton quenching to the ultrafast electron transfer from the photoexcited PbS QDs to TMPyP, which is expected to generate TMPyP anion radical species ($TMPyP^{\cdot-}$) with a characteristic broad peak between 700 and 800 nm.[31,32] By monitoring the fs-TA in the visible region for both small and large QDs, we deciphered the signal for electron injection from the photo-excited PbS QDs to TMPyP through the evolution of $TMPyP^{\cdot-}$, with a temporal resolution of approximately 120 fs (Figure S6, Supporting Information). The ultrafast electron injection to TMPyP as inferred from the formation of its anionic species, and the ultrafast CR as inferred from the ultrafast GSB recovery, are further indications of the ground-state complexation and subsequent static CT between the TG-capped PbS QDs and cationic porphyrin. This could also indicate that the molecular acceptor is likely to be adsorbed on the surface of QDs which is consistent with previous reports.[4,8,9]

Figure 4 shows a comparison of the kinetic traces extracted from the GSB feature within the fs-TA spectra of different PbS QD sizes upon the addition of a fixed [TMPyP]. The dynamics were fit to double-exponential functions with time constants of a few to tens of picoseconds, and tens to hundreds of picoseconds. The two observed components suggest the occurrence of two

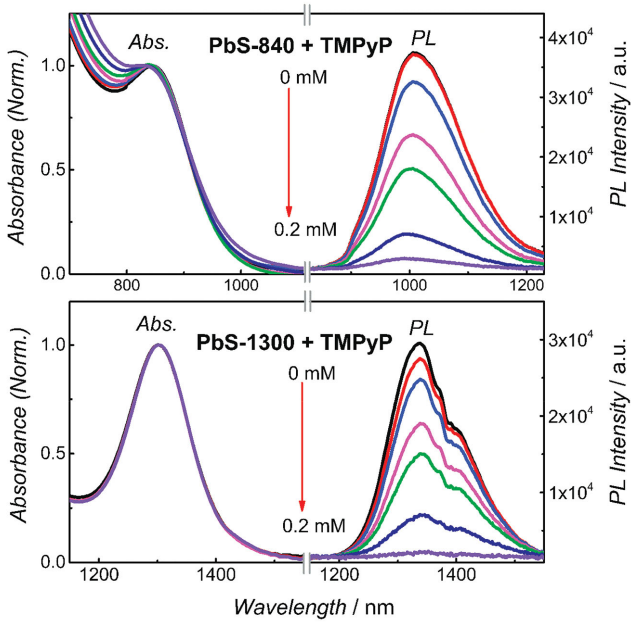

Figure 2. Steady-state absorption and PL (λ_{ex} = 700 nm and λ_{ex} = 1000 nm, respectively) spectra of PbS-840 and PbS-1300 upon the addition of different [TMPyP], in DMSO-d_6. The green traces signify the addition of 0.08×10^{-3} M TMPyP.

types of donor–acceptor ion pairs with different associated couplings, in accordance with previous reports on other donor–acceptor systems.[11,33,34] The fittings for the bleach recoveries of PbS-840, PbS-1000, and PbS-1300 indicate that not only is the percentage recovery greater for smaller PbS QDs, but the rate of CR is also enhanced with the smaller QD size. For instance, the recovery time constants due to carrier recombination for PbS-840 are 7.4 and 87.5 ps at 0.1×10^{-3} M TMPyP, and they elongate to 25.8 and 572.2 ps for PbS-1300 with similar [TMPyP], thus indicating that the CR varies strongly as a function of QD size. The differences in the recombination rates/percentages indicate variation in the CT rates between various QD sizes and TMPyP. In addition, the system reveals a clear dependence not only on the free energy driving force between the donor and acceptor units[35] (Figure S3B, Supporting Information); but also on the presence of the charged molecular acceptors. Because of their increased bandgaps, smaller QDs are expected to have more favorable CB energies for injecting electrons into TMPyP. Notably, although we did not measure the GSB recovery kinetics for PbS-1550 because of a lack of sufficient white light in this region within our TA setup, the steady-state PL spectra (Figure S4, Supporting Information) provide sufficient evidence for the CT to TMPyP.

To explore the possibility of electron transfer through the diffusion-controlled process, we employed nanosecond TA spectroscopy to demonstrate that TMPyP quenches the excited state of the large QDs on the microsecond time scale (Figure 3B and **Figure 5**). The exciton quenching on the nanosecond-to-microsecond time scales is due to a dynamic mechanism, whereby collisionally gated CT occurs between the QDs and freely diffusing TMPyP molecules. This observation provides further evidence for the involvement of both static and dynamic mechanisms in describing the overall quenching process, in agreement with other reported QD/molecular acceptor systems.[8,36] The results of the nanosecond TA studies were consistent with the results of the PL quenching measurements, as shown in Figure 5 and 2, respectively. The nanosecond TA studies revealed that the addition of 0.08×10^{-3} M TMPyP resulted in the evolution of a new fast decay component and maintenance of approximately 67% of the QD population with an elongated lifetime of 0.98 µs. Similarly, the PL quenching measurements revealed that, upon the addition of 0.08×10^{-3} M TMPyP to PbS-1300 (green traces), approximately 64% of the QD population maintained an active PL.

2.3. The Importance of Interfacial Electrostatic Interaction

We argue that, although the CT from PbS QDs to TMPyP is facilitated by their interfacial band energy level alignment, this CT is based primarily on the prior availability of intimate contact

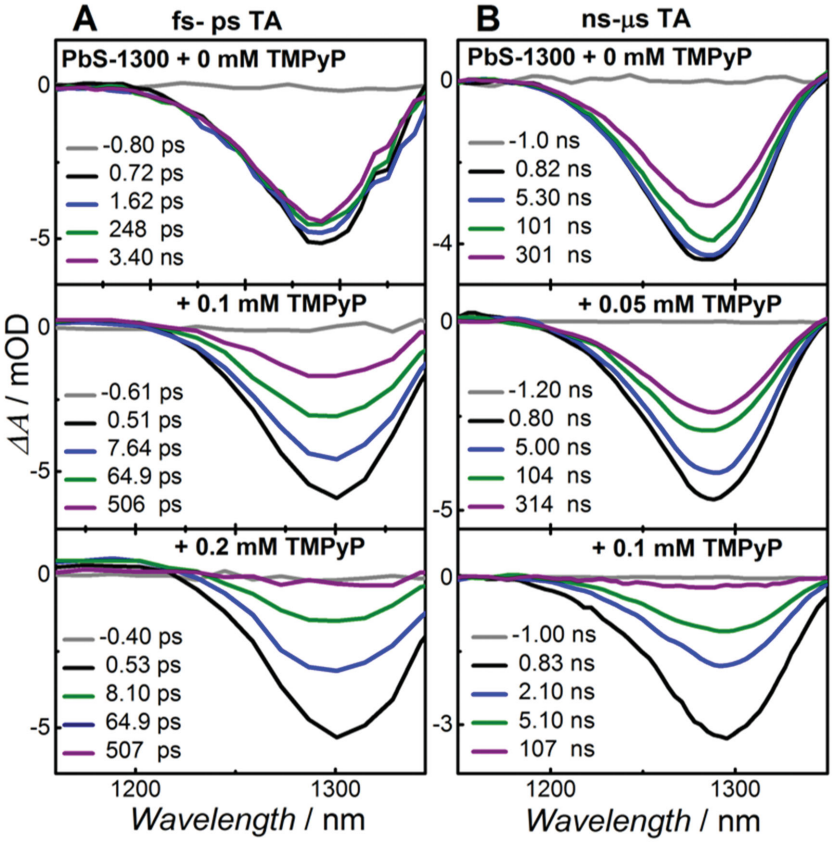

Figure 3. A) fs-ps TA and B) ns-µs TA spectra of PbS-1300 upon the addition of different [TMPyP], with $\lambda_{ex} = 1.3E_g$ in DMSO-d_6.

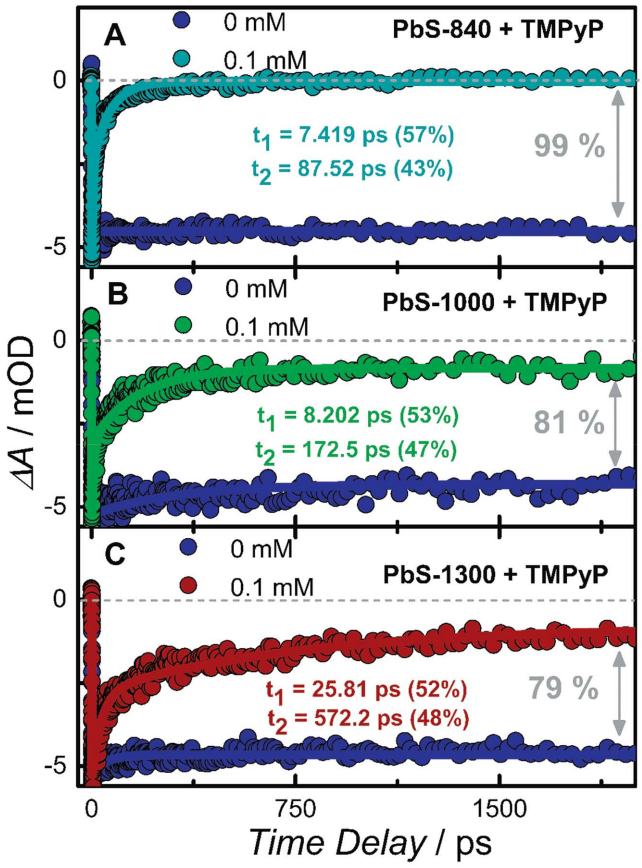

Figure 4. fs-TA kinetics traces at the GSB of PbS QDs with different sizes upon the addition of 0.1×10^{-3} M TMPyP, with $\lambda_{ex} = 1.3E_g$ in DMSO-d_6. The presented data (A, B, and C) represent QD samples PbS-840, PbS-1000, and PbS-1300, respectively.

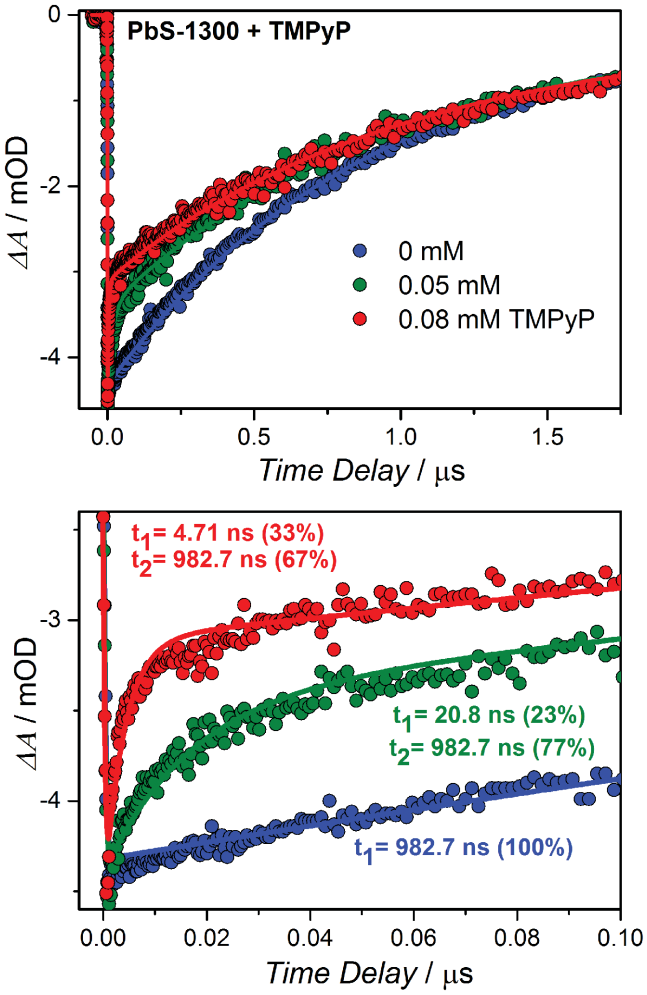

Figure 5. ns-μs TA kinetics at the GSB for PbS-1300 with λ_{ex} = 900 nm, in the long time-scale (top). Upon TMPyP addition, a double exponential function arises as clarified in the short-time window (bottom). By fixing t_1 value to the lifetime of pure QDs (982.7 ns), it is clarified that its amplitude decreases upon TMPyP addition.

through the electrostatic interaction between the two moieties as an additional driving force. To confirm this hypothesis, we evaluated the interaction between PbS QDs and a neutrally charged free-base porphyrin, 5,10,15,20-tetra(4-pyridyl)porphyrin (TPyP), under the same experimental conditions. In this case, whereas TPyP has energy levels similar to those of TMPyP,[35,37] it lacks the positive charges that provide electrostatic interaction with the TG-capped QDs. **Figure 6** shows that the addition of TPyP to PbS-1300 did not induce any PL quenching, nor significantly change the fs-TA kinetics. The complete absence of PL quenching between large PbS QDs and TPyP, and the lack of any differences in the QDs' lifetime upon TPyP addition (Figure S7, Supporting Information), reveal the importance of electrostatic interaction as a key parameter in controlling the CT at QD interfaces and in providing a broader effective QD size range.

Moreover, the importance of the electrostatic interaction would be manifested if it can also facilitate CT at interfaces with a dis-favorable energy level alignment. Accordingly, we perform another control experiment for measuring the PL quenching upon the addition of an equally charged molecule that provides a dis-favorable energy level alignment with PbS QDs. For that purpose, we use ZnTMPyP, since the complexation of Zn^{+2} with porphyrin had been reported to induce a rise in the porphyrin LUMO level by ≈1.5 eV;[38] which should greatly inhibit CT from the QDs to the porphyrin species. Interestingly, complete PL quenching was recorded with three QD sizes (PbS-800, PbS-1300, and PbS-1500) upon the addition of ZnTMPyP (Figure S9, Supporting Information), which suggests that the proximity of a cationic species could enhance charge transfer even with a slight dis-favorable-energy level alignment.

3. Conclusion

In summary, we report, for the first time, the possibility of extending the effective size range for CT at the PbS QDs interface, thus allowing the coupling of the faster electron injection rate of small QDs and the greater absorption range of large QDs to harvest different portions of the broad solar spectrum, overcoming one of the greatest challenges impeding the development of PbS QD-based solar cells. More specifically, we demonstrate that, by utilizing both the quantum confinement and the interfacial electrostatic interaction, one can now extend the effective QD size for

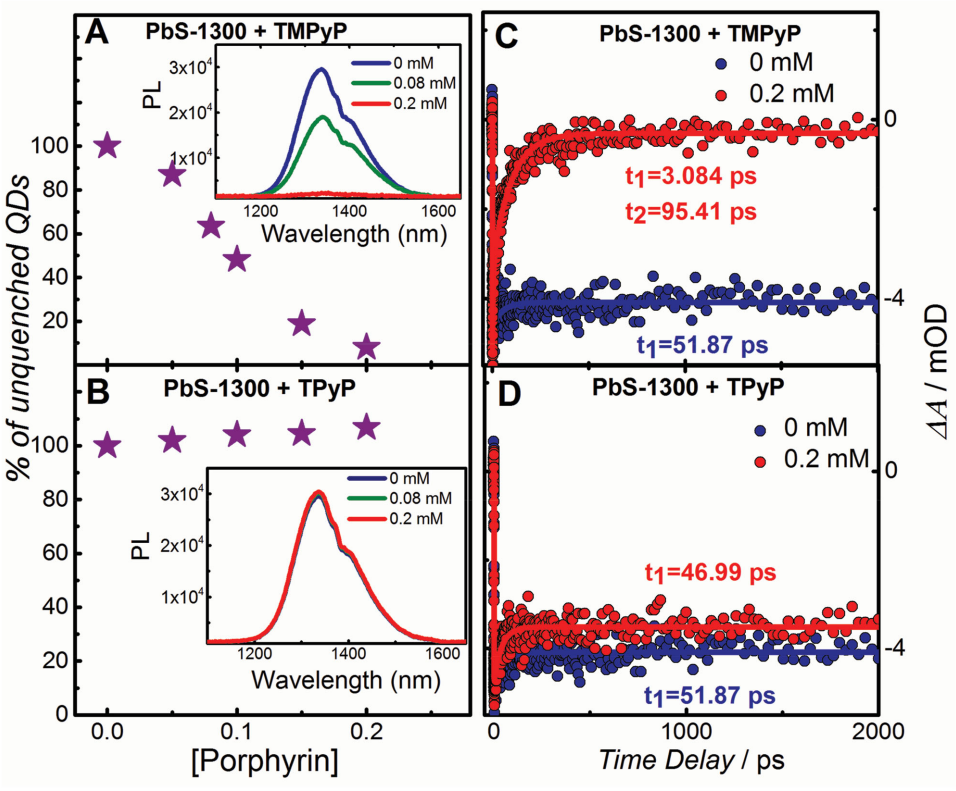

Figure 6. Plots of the percentage of unquenched QDs upon the addition of A) TMPyP and B) TPyP, where the insets show the representative PL spectra. fs-TA kinetics at the GSB for PbS-1300 upon the addition of C) TMPyP and D) TPyP.

CT to include most of the near-infrared spectral region, reaching beyond the previously reported cut-off CT bandgaps for PbS QDs. We believe that these findings shed light on the key variable components for designing QD-sensitized solar cells as well as other state-of-the-art devices that rely on interfacial CT processes.

4. Experimental Section

Quantum Dot Synthesis: The QD synthesis was performed in a three-neck round bottom flask with Schlenk line setting using lead oleate and TMS as precursors in ODE, according to Hines and Scholes.[39] The TMS injection temperature was varied between 120–67 °C depending on the required QD size. After TMS injection, slow cooling was allowed to facilitate size focusing and help narrowing the size distribution. Once 60 °C was reached, $CdCl_2$ treatment ($CdCl_2$-TDPA-Oleylamine) was introduced according to Ip et al.[5] Slow cooling was continued until 35 °C is reached whereby acetone was added to precipitate the QDs from solution. After centrifugation, the OA-capped $CdCl_2$-treated PbS QDs were purified twice by dispersion in toluene and reprecipitation with acetone/methanol (1:1 volume ratio), and finally dissolved in octane (150 mg mL^{-1}).

Solution-Phase Ligand Exchange: The solution-phase ligand exchange was done according to a modified literature method.[22] Shortly, 100 µL of the OA-capped $CdCl_2$-treated QDs (150 mg mL^{-1}) were dispersed in 4 mL of octane. The mixture was added to a solution of TG (90 µL, 0.112 g) in DMSO (4 mL). The biphasic system was vortexed vigorously for 30 seconds, resulting in the migration of QDs from nonpolar to polar phase. After centrifugation at 5000 rpm for 1 min, the polar phase was separated from the clear nonpolar phase. The polar QD dispersion was rinsed four more times with an equal volume of octane, followed by vortexing, and centrifugation. Finally, acetonitrile was added in 4:1 volume ratio to induce precipitation and remove excess ligands, followed by centrifugation, and isolation. The TG-capped $CdCl_2$-treated QDs were then dried under vacuum overnight, dispersed in DMSO, and centrifuged at 15 000 rpm for 5 min to remove any aggregates.

Transmission Electron Microscopy (TEM): This was carried out on a TitanG2 80–300 instrument, FEI Co., Super Twin, x-FEG, operating at 300 kV. The PbS QDs dispersions in DMSO were deposited onto 300 mesh gold grids with holey carbon film, and dried in air for at least 4 h before imaging.

Dynamic Light Scattering (DLS) and Zeta-Potential: The measurements were performed using a Zetasizer Nano (Malvern) at 20 °C in a 1 cm path length quartz cuvette, with back-scattering and front-scattering detection modes, respectively. The size distributions are based on the hydrodynamic diameter of the QD dispersions in DMSO.

Photoelectron Spectroscopy: X-ray photoelectron spectroscopy (XPS) measurements were carried out in an ultrahigh vacuum chamber (UHV) Omicron chamber equipped with a SPHERA U7 hemispherical energy analyzer, using X-ray photons with an incident kinetic energy of 1486.6 eV from a monochromated Al K α X-ray source with a total energy resolution of 0.1 eV. The survey spectrum was acquired at a pass energy of 40 eV, while the high resolution core level peaks for the various elements were obtained at a pass energy of 20 eV. The photoelectrons were collected by the SPHERA U7 hemispherical energy analyzer with a 7 channel MCD detector, in Constant Analyzer Energy (CAE) mode. The spectra were referenced to the C1s core level peak with its C–C chemical bond component neutralized at 285.0 eV. The QD dispersions in DMSO were deposited on tin-doped indium oxide (ITO) coated glass by drop-casting, followed by mild heating at 35 °C to accelerate the drying process. As for ultraviolet photoelectron spectroscopy (UPS) measurements, the base pressure was maintained below 5×10^{-9} mb. He I photons (21.2 eV) were used to acquire the spectra at normal emission. The photon line width was ≈250 eV and the minimum spot size was ≈1 mm.

Steady-State Quenching Measurements: The stock TG-capped $CdCl_2$-treated PbS QDs were diluted with extra DMSO to maintain a constant concentration (≈1.5×10^{-6} M), as determined by the optical density (OD) at the first exciton absorption peak (i.e., $1S_h \rightarrow 1S_e$ transition) within a 1 cm path length quartz cuvette, where $\varepsilon_{pbs\ QD} = 19600 * r^{2.32}$.[40] Alternatively, the stock solutions were diluted with different concentrations of the porphyrin (TPyP or TMPyP in DMSO) while maintaining a fixed QDs concentration. The steady-state absorption spectra of these solutions were measured using a Cary 5000 UV–vis-NIR spectrophotometer (Varian Inc.), while the steady-state photoluminescence spectra were measured using a Jobin–Yvon–Horiba Nanolog spectrofluorometer.

Transient Absorption (TA) Spectroscopy: The stock PbS QDs were diluted with extra DMSO, or alternatively porphyrin (TPyP or TMPyP) in DMSO, while maintaining a fixed QD concentration (≈1.5×10^{-6} M) as determined by the OD at the first exciton absorption peak within a 2 mm path length cuvette, where $\varepsilon_{pbs\ QD} = 19600 \times r^{2.32}$.[40] All TA experiments were conducted at room temperature, with constant sample stirring to avoid the photocharging of QDs.[41,42] The absorption spectrum of each sample measured before and after TA experiments did not show any degradation. Further TA setup details were published elsewhere[43] and are also available in the Supporting Information.

Supporting Information

Supporting Information is available from the Wiley Online Library or from the author.

Acknowledgements

The work reported here was supported by King Abdullah University of Science and Technology (KAUST). A. O. El-Ballouli gratefully acknowledges Dr. Ahmed L. Abdelhady for his assistance with TEM measurements.

Received: September 22, 2015
Revised: October 8, 2015
Published online: November 17, 2015

[1] A. Hagfeldt, M. Graetzel, *Chem. Rev.* **1995**, *95*, 49.
[2] J. B. Sambur, T. Novet, B. A. Parkinson, *Science* **2010**, *330*, 63.
[3] W. A. Tisdale, K. J. Williams, B. A. Timp, D. J. Norris, E. S. Aydil, X. Y. Zhu, *Science* **2010**, *328*, 1543.
[4] A. O. El-Ballouli, E. Alarousu, A. Usman, J. Pan, O. M. Bakr, O. F. Mohammed, *ACS Photonics* **2014**, *1*, 285.
[5] A. H. Ip, S. M. Thon, S. Hoogland, O. Voznyy, D. Zhitomirsky, R. Debnath, L. Levina, L. R. Rollny, G. H. Carey, A. Fischer, K. W. Kemp, I. J. Kramer, Z. Ning, A. J. Labelle, K. W. Chou, A. Amassian, E. H. Sargent, *Nat. Nanotechnol.* **2012**, *7*, 577.
[6] C.-H. M. Chuang, P. R. Brown, V. Bulovic, M. G. Bawendi, *Nat. Mater.* **2014**, *13*, 796.
[7] J. Pan, A. O. El-Ballouli, L. Rollny, O. Voznyy, V. M. Burlakov, A. Goriely, E. H. Sargent, O. M. Bakr, *ACS Nano* **2013**, *7*, 10158.
[8] K. E. Knowles, M. Malicki, E. A. Weiss, *J. Am. Chem. Soc.* **2012**, *134*, 12470.
[9] K. E. Knowles, M. Malicki, R. Parameswaran, L. C. Cass, E. A. Weiss, *J. Am. Chem. Soc.* **2013**, *135*, 7264.
[10] Y. Yang, W. Rodriguez-Cordoba, T. Lian, *J. Am. Chem. Soc.* **2011**, *133*, 9246.
[11] A. O. El-Ballouli, E. Alarousu, M. Bernardi, S. M. Aly, A. P. Lagrow, O. M. Bakr, O. F. Mohammed, *J. Am. Chem. Soc.* **2014**, *136*, 6952.
[12] J. J. Choi, W. N. Wenger, R. S. Hoffman, Y.-F. Lim, J. Luria, J. Jasieniak, J. A. Marohn, T. Hanrath, *Adv. Mater.* **2011**, *23*, 3144.
[13] X. Wang, G. I. Koleilat, J. Tang, H. Liu, I. J. Kramer, R. Debnath, L. Brzozowski, D. A. R. Barkhouse, L. Levina, S. Hoogland, E. H. Sargent, *Nat. Photonics* **2011**, *5*, 480.
[14] I. J. Kramer, L. Levina, R. Debnath, D. Zhitomirsky, E. H. Sargent, *Nano Lett.* **2011**, *11*, 3701.
[15] B.-R. Hyun, Y.-W. Zhong, A. C. Bartnik, L. Sun, H. D. Abruna, F. W. Wise, J. D. Goodreau, J. R. Matthews, T. M. Leslie, N. F. Borrelli, *ACS Nano* **2008**, *2*, 2206.
[16] H. C. Leventis, F. O'Mahony, J. Akhtar, M. Afzaal, P. O'Brien, S. A. Haque, *J. Am. Chem. Soc.* **2010**, *132*, 2743.
[17] A. Gocalinska, M. Saba, F. Quochi, M. Marceddu, K. Szendrei, J. Gao, M. A. Loi, M. Yarema, R. Seyrkammer, W. Heiss, A. Mura, G. Bongiovanni, *J. Phys. Chem. Lett.* **2010**, *1*, 1149.
[18] H. Zhao, H. Liang, B. A. Gonfa, M. Chaker, T. Ozaki, P. Tijssen, F. Vidal, D. Ma, *Nanoscale* **2014**, *6*, 215.
[19] A. Guchhait, A. K. Rath, A. J. Pal, *Sol. Energy Mater. Sol. Cells* **2011**, *95*, 651.
[20] L. Tao, Y. Xiong, H. Liu, W. Shen, *Nanoscale* **2014**, *6*, 931.
[21] Z. Li, C. M. Wang, L. Persaud, T. E. Mallouk, *J. Phys. Chem.* **1988**, *92*, 2592.
[22] A. Fischer, L. Rollny, J. Pan, G. H. Carey, S. M. Thon, S. Hoogland, O. Voznyy, D. Zhitomirsky, J. Y. Kim, O. M. Bakr, E. H. Sargent, *Adv. Mater.* **2013**, *25*, 5742.
[23] K. Katsiev, A. H. Ip, A. Fischer, I. Tanabe, X. Zhang, A. R. Kirmani, O. Voznyy, L. R. Rollny, K. W. Chou, S. M. Thon, G. H. Carey, X. Cui, A. Amassian, P. Dowben, E. H. Sargent, O. M. Bakr, *Adv. Mater.* **2014**, *26*, 937.
[24] W. Feng, C. Qin, Y. Shen, Y. Li, W. Luo, H. An, Y. Feng, *Sci. Rep.* **2014**, *4*, 3777/1.
[25] D. Wang, H. Zhao, N. Wu, El M. A. Khakani, D. Ma, *J. Phys. Chem. Lett.* **2010**, *1*, 1030.
[26] P. R. Brown, D. Kim, R. R. Lunt, N. Zhao, M. G. Bawendi, J. C. Grossman, V. Bulovic, *ACS Nano* **2014**, *8*, 5863.
[27] J. R. Lakowicz, *Principles of Fluorescence Spectroscopy*, 3rd ed., Springer, New York **2006**.
[28] M. Idowu, E. Lamprecht, T. Nyokong, *J. Photochem. Photobiol., A* **2008**, *198*, 7.
[29] V. I. Klimov, *J. Phys. Chem. B* **2000**, *104*, 6112.
[30] B. C. Fitzmorris, Y.-C. Pu, J. K. Cooper, Y.-F. Lin, Y.-J. Hsu, Y. Li, J. Z. Zhang, *ACS Appl. Mater. Interfaces* **2013**, *5*, 2893.
[31] M. Kumar, P. Neta, T. P. G. Sutter, P. Hambright, *J. Phys. Chem.* **1992**, *96*, 9571.
[32] S. M. Aly, S. Goswami, Q. A. Alsulami, K. S. Schanze, O. F. Mohammed, *J. Phys. Chem. Lett.* **2014**, *5*, 3386.
[33] O. F. Mohammed, K. Adamczyk, N. Banerji, J. Dreyer, B. Lang, E. T. J. Nibbering, E. Vauthey, *Angew. Chem., Int. Ed.* **2008**, *47*, 9044.
[34] O. F. Mohammed, E. Vauthey, *J. Phys. Chem. A* **2008**, *112*, 5804.
[35] K. Zhu, X. Hu, Q. Ge, Q. Sun, *Anal. Chim. Acta* **2014**, *812*, 199.
[36] S. Mandal, M. Rahaman, S. Sadhu, S. K. Nayak, A. Patra, *J. Phys. Chem. C* **2013**, *117*, 3069.
[37] Y. Ohmori, E. Itoh, K. Miyairi, *Thin Solid Films* **2006**, *499*, 369.
[38] M.-S. Liao, S. Scheiner, *J. Comput. Chem.* **2002**, *23*, 1391.
[39] M. A. Hines, G. D. Scholes, *Adv. Mater.* **2003**, *15*, 1844.
[40] L. Cademartiri, E. Montanari, G. Calestani, A. Migliori, A. Guagliardi, G. A. Ozin, *J. Am. Chem. Soc.* **2006**, *128*, 10337.
[41] S. J. O. Hardman, D. M. Graham, S. K. Stubbs, B. F. Spencer, E. A. Seddon, H.-T. Fung, S. Gardonio, F. Sirotti, M. G. Silly, J. Akhtar, P. O'Brien, D. J. Binks, W. R. Flavell, *Phys. Chem. Chem. Phys.* **2011**, *13*, 20275.
[42] M. C. Beard, K. P. Knutsen, P. Yu, J. M. Luther, Q. Song, W. K. Metzger, R. J. Ellingson, A. J. Nozik, *Nano Lett.* **2007**, *7*, 2506.
[43] J. Sun, W. Yu, A. Usman, T. T. Isimjan, S. DGobbo, E. Alarousu, K. Takanabe, O. F. Mohammed, *J. Phys. Chem. Lett.* **2014**, *5*, 659.